Highly Surface-Textured ZnO:Al Films Fabricated by Controlling the Nucleation and Growth Separately for Solar Cell Applications

Dongyun Wan, Fuqiang Huang,* and Yaoming Wang

CAS Key Laboratory of Materials for Energy Conversion, Shanghai Institute of Ceramics, Chinese Academy of Sciences, Shanghai 200050, People's Republic of China

Xinliang Mou and Fangfang Xu

Inorganic Materials Analysis and Testing Center, Shanghai Institute of Ceramics, Chinese Academy of Sciences, Shanghai 200050, People's Republic of China

ABSTRACT Highly surface-textured ZnO:Al (AZO) thin films have been fabricated at room temperature by a two-step magnetron sputtering process and using an oxygen-deficient ZnO target with small grain sizes. The as-deposited AZO films are composed of a highly oriented seed layer and a closely packed columnar overlayer with pyramidal growth fronts, supporting a two-step mechanism of crystallite nucleation and grain growth. The structural, optical, and electrical properties of the AZO films can be tuned by the deposition conditions. The optimal two-step AZO film with a maximum root-mean-square roughness of 40.2 nm reaches a very low square resistance of 0.66 Ω/sq ($\rho = 1.32 \times 10^{-4}\ \Omega \cdot$ cm) with an average transparency of 87.9% in the range of 400−1100 nm. The maximum haze factor of the as-deposited film is 60.7% at 360 nm, and the average haze factor is 14.8%. These properties are comparable to or exceed the reported values of surface-textured SnO_2- and ZnO-based transparent conducting oxide films, making our films suitable for transparent electrode applications, especially in thin-film solar cells.

KEYWORDS: ZnO:Al thin films • transparent conducting oxide • surface-textured • two-step sputtering • thin-film solar cells

1. INTRODUCTION

ZnO-based transparent conducting oxide (TCO) films, used as a front electrode in solar cells, have attracted significant attention because of their low cost and nontoxicity (1, 2). Surface-textured ZnO films with incident-light-capturing ability have become an important issue to improve the photovoltaic efficiency for a-Si/μc-Si and CIGS thin-film solar cells (3−5). For a-Si:H and μc-Si:H solar cells, relatively low optical absorption coefficients in the red and near-IR spectral ranges have been observed because of the indirect-transition nature in elemental silicon. A textured rough surface of the TCO layers can improve the performance by allowing efficient light scattering inside the solar cell and, hence, more light absorption along the longer scattering path. Therefore, surface-texture techniques have received much interest and are becoming an industrial practice in the a-Si/nc-Si and μc-Si solar cells.

There are two main surface-textured ZnO film deposition methods. Neither low-pressure chemical vapor deposition (LPCVD) (6−8) nor a postdeposition etching process after magnetron sputtering (9−15) is ideal for forming quality-stable ZnO films because of difficult process control. The high deposition temperature of 200−500 °C for magnetron-sputtered ZnO films is also deleterious to the device performance (11, 16, 17). Therefore, there is an urgent demand for developing a new low-cost technique to produce high-quality surface-textured ZnO films.

A new film deposition mechanism is investigated here for the fabrication of surface-textured ZnO films by using widely used magnetron sputtering. In general, the combined nucleation/growth film deposition is divided into two individual steps, including crystallite nucleation and grain growth. The fast growth of the overlayer in the second step without further nucleation of new grains can facilitate the generation of large columnar grains with a textured surface on a highly oriented crystallite (seed) layer deposited in the first step.

The conventional ZnO film deposition is a simultaneous process of nucleation/growth, with the ZnO grains oriented along the [001] direction. Under fixed sputtering conditions, the kinetic energy and concentration of sputtered atoms on the substrate are constant and result in a corresponding microstructure (grain size, surface texture, etc.). A small amount of low-kinetic-energy atoms on the substrate with low mobility is not able to grow a large-grain, surface-textured film. Although larger grains can be obtained from improving the kinetic energy of sputtered atoms by heating the substrate, the high-temperature film deposition is troublesome for solar device fabrication. Except for the high kinetic energy of sputtered atoms, a highly textured surface requires

* To whom correspondence should be addressed. E-mail: huangfq@mail.sic.ac.cn.
Received for review May 12, 2010 and accepted June 21, 2010

DOI: 10.1021/am100416e
2010 American Chemical Society

ARTICLE

a high concentration of atoms on the substrate for a fast growth stage. Enough sputter power and material supply are essential to ensure large grains, but the fast growth of the overlayer only on a highly oriented crystallite (seed) layer might form a highly textured surface. Normally, a small-grain seed layer crystallizes from a low kinetic energy and a low concentration of sputtered atoms in the first step, and the following fast growth with a high kinetic energy and a high concentration of atoms favors the selection of the fastest growing grains on the seed layer. Some seeds grow up rapidly into very large columnar grains; the others are crowded out in the competition, and advancing faceted fronts of the remaining grains around the [001] axis finally form a pyramidal microstructure on the surface.

On the basis of the proposed mechanism, we report a simple technique to fabricate surface-textured Al-doped ZnO (AZO) films at room temperature using magnetron sputtering only. The technique involves a two-step deposition process with a homemade Zn-rich AZO target. In the two-step process, a "seed" layer was first formed on the substrate to guide the subsequent growth of a well-crystallized AZO film. The surface texture of the AZO films is next tuned by adjusting the deposition condition in the second step. The film reaches a very low square resistance of 0.66 Ω/sq and an average transmittance of 87.9% in the range of 400−1100 nm, comparable to or exceeding the best reported values of indium−tin oxide, FTO, and ZnO-based TCO films (17, 18).

2. EXPERIMENTAL SECTION

The ZnO:Al (AZO) powder precursor was prepared by coprecipitation using an aqueous solution with a 98:2 molar ratio of $Zn(CH_3COO)_2 \cdot 2H_2O$ (analytical reagent) and $Al(NO_3)_3 \cdot 9H_2O$ (analytical reagent) with an ammonia solution. The precipitate was ball-milled for 12 h with the additive of 0.25 mol % zinc fine powders (0.1−4 μm, 5 N) based on the total metal elements (Zn + Al). The uncalcined mixed powders were die-pressed into a green body and then sintered in air at 850 °C for 3 h for the final AZO target.

The AZO films were deposited in a JPG450 magnetron sputtering system on glass slides. Films were prepared using both a commercial target and the homemade target described above. An unthrottled base pressure of 2.0×10^{-4} Pa was reached using a combined vacuum system of mechanical and turbomolecular pumps. All of the experiments were conducted at nominal room temperature (with the maximum temperature monitored being 55 °C) and under a flow of high-purity argon gas (99.99%, 15 sccm). Because the AZO target is electrically conducting, direct-current (dc) sputtering was used in this work. The two-step deposition procedure involves a first deposition of a thin AZO layer as a "seed" layer, followed by a second deposition to grow a textured film. For this purpose, a lower dc power (60 W) at a higher pressure (1.2 Pa) was used in the first step, while a higher power (100−140 W) at a lower pressure (0.2 Pa) was used in the second step. In addition, the power of the second step was varied from 80 to 140 W to examine its effect on the electrical and optical properties of the textured films.

X-ray diffraction (XRD) measurements were carried out on a Bruker AXS D8 Advance diffractometer using Cu Kα radiation to characterize the crystallization and phase structure of the films. Surface and cross-sectional morphologies of the AZO powder, targets, and films were investigated by scanning electron microscopy (SEM; JEOL 6510), field-emission SEM (LEO-1530VP), and transmission electron microscopy (TEM; JEM2100F). Atomic force microscopy (AFM; Seiko II SPI3800 V and spa300HV) and a profilometer (Dektak 150) were used to evaluate the roughness and thickness of the AZO films. The van der Pauw method was used with an Accent HL5500 instrument to measure the electrical transport properties including the resistivity, carrier concentration, and Hall mobility. UV−visible−IR transmission spectra of the films were recorded by a spectrophotometer (Hitachi UV-3010PC) between 300 and 1200 nm. The absorption spectra reported were obtained after subtraction of the signal of the glass substrate.

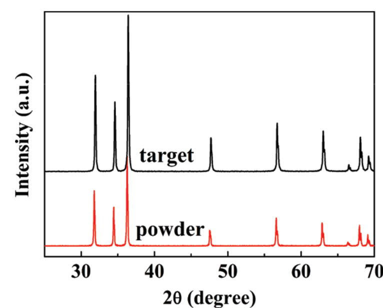

FIGURE 1. XRD patterns of the AZO powders and target.

3. RESULTS AND DISCUSSION

3.1. Effects of the Sputtering Target.

The as-prepared AZO powders were obtained from coprecipitation, and the AZO target was sintering from such powders with the addition of excess zinc. The XRD patterns and SEM images of the as-prepared AZO powders and the ceramic AZO target are shown in Figures 1 and 2, respectively. The diffraction peaks of the target have shifted to higher angles, indicating a significant contraction of the unit cell during sintering. The particle dimensions in the platelike AZO powders range from 0.2 to 2.0 μm, while the polyhedral grains in the ceramic target are about 1−3 μm. The density of the 850 °C sintered target is comparable with that of the commercial target sintered at 1300−1400 °C, over 95% of the theoretical value, but our target has finer grains, according to the SEM images, presumably because of finer powders and a lower sintering temperature. The low-melting metallic zinc powders were used as the sintering agent during the low-temperature densification of the ceramic target. As a side effect of the addition of excess zinc, the resistance of the homemade AZO target reduced to less than 1.0 Ω/sq, lower than 3.0−7.0 Ω/sq of the commercial AZO targets with the same Al doping level.

The advantages of the homemade target are manifested in the property of the films made using (one-step) dc sputtering, typically at 100 W under 0.2 Pa of argon pressure for 30 min. A lower square resistance of 4.9 Ω/sq was observed for the films made from the homemade target, compared with 7.4 Ω/sq of the commercial one. The films have different morphologies, as depicted by the SEM and AFM images in Figure 3. The film obtained from the homemade target has a much rougher textured surface than that from the commercial one, in good agreement with the corresponding root-mean-square (rms) roughness values of 14.2 and 5.34 nm, as listed in Table 1. Their optical properties are also remarkably different, as shown in Figure 4.

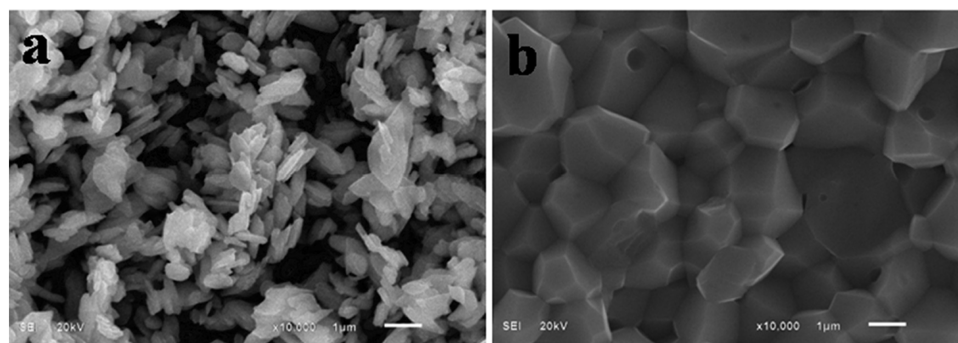

FIGURE 2. SEM images of (a) the AZO powders and (b) the 850 °C sintered target.

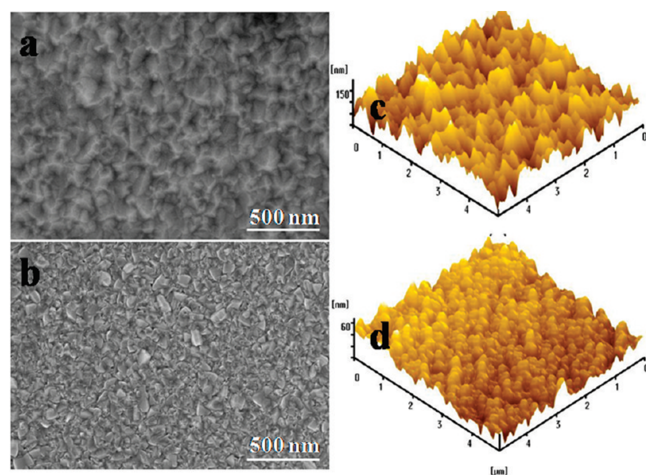

FIGURE 3. SEM and AFM images of one-step 100-W-deposited AZO films obtained from (a and c) the homemade target and (b and d) the commercial target.

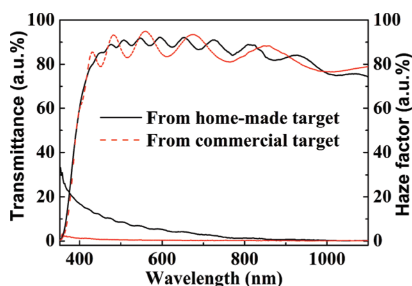

FIGURE 4. Transmittance and haze spectra of one-step 100-W-deposited AZO films obtained from the homemade target (solid lines) and the commercial target (dashed lines).

Although the transmission is similar, the haze factor, which is the ratio of the diffuse to total transmission commonly used to indicate the light-capturing ability of a surface-textured film, is much higher in the film made from the homemade target (28% at 360 nm vs 2.3% at the same wavelength). As shown in Table 1, overall, the films from

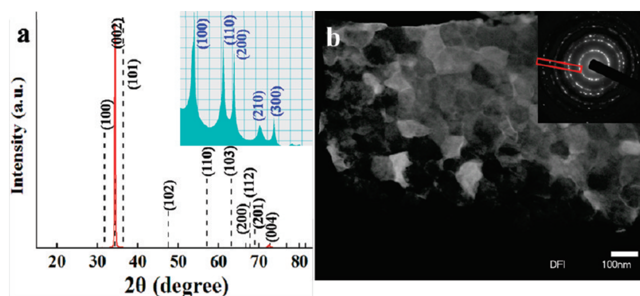

FIGURE 5. (a) XRD patterns of the seed AZO layer (red lines) and the black dashed lines from JCPDS No. 01-1136 and (b) ADF image of the 60-W-deposited seed layer. The SAED pattern and its profile image are displayed in the top right insets of parts b and a.

the homemade target also have superior electrical properties compared to those from the commercial one.

3.2. Effects of Two-Step Sputtering.

Our two-step deposition process was developed to promote seeding in the first layer, followed by textured growth in the overlayer. To aid crystal nucleation, a much lower power (60 W), together with a higher base pressure (1.2 Pa), was used in the first step to reduce the kinetic energy and ion flux, which presumably could allow more time for surface diffusion and crystallization. The seed layer examined by SEM and TEM shows a thickness of about 200−300 nm, as shown in Figure 5 (also see later in Figure 9, the cross-sectional micrograph containing both the seed layer and the columnar overlayer). The XRD pattern (Figure 5a, red solid lines) suggests a strong (001) texture, as evidenced by the only two diffraction peaks, indexed as (002) and (004) reflections; all other reflections of the zinc blende structure (JCPDS No. 01-1136 shown in black dashed lines) are absent. The inset of Figure 5b shows a small area electron diffraction (SAED) pattern that has a ringlike distribution, indicating no in-plane texture between the [001]-oriented grains seen in their annular dark-field image in Figure 5b. The (001) texture is also consistent with the intensity profile of the SAED pattern shown in the inset

Table 1. Physical Properties of One-Step Sputtered AZO Films Obtained from the Homemade Target and the Commercial Target

sample	thickness (μm)	rms roughness (nm)	haze at 360 nm (%)	growth temperature (K)	$R_{\square}$ (Ω/sq)	ρ ($\times 10^{-4}$ $\Omega \cdot$ cm)	μ (cm^2/V $\cdot$ s)	N ($\times 10^{21}$ cm^{-3})
0.2 Pa/100 W/30 min (homemade target)	1.26 ± 0.03	14.2 ± 0.3	27.8 ± 0.41	RT	4.94 ± 0.16	3.55 ± 0.09	9.56 ± 0.18	1.84 ± 0.12
0.2 Pa/100 W/30 min (commercial target)	1.21 ± 0.02	5.34 ± 0.12	2.3 ± 0.05	RT	7.43 ± 0.27	8.89 ± 0.17	5.98 ± 0.08	1.17 ± 0.05

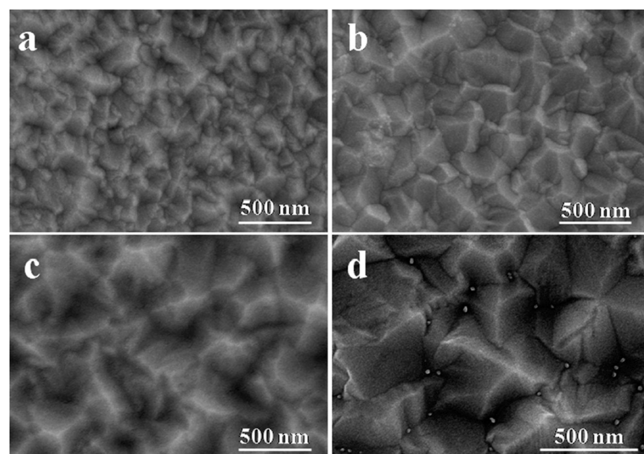

FIGURE 6. SEM images of two-step sputtered AZO films deposited with different supplied powers: (a) 80 W, (b) 100 W, (c) 120 W, and (d) 140 W, respectively.

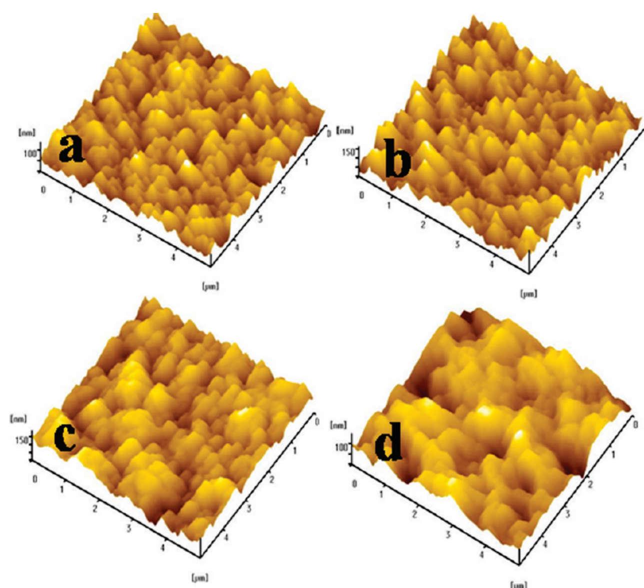

FIGURE 7. AFM images of two-step sputtered AZO films deposited with different supplied powers, revealing differences in the grain size and morphology: (a) 80 W, (b) 100 W, (c) 120 W, and (d) 140 W, respectively.

of Figure 5a, which contains only (*hk*0) lattice planes. Note also that these seed crystals have apparently covered the entire substrate surface because the grains in Figure 5b appear to be contiguous and closely packed.

This highly oriented and closely packed seed layer provides an excellent substrate to grow a well-crystallized overlayer of the desired thickness. The overlayer was deposited at a higher power (80−140 W) and a lower pressure (0.2 Pa) to facilitate faster film growth without further nucleation of new grains. SEM and AFM images of the as-sputtered sample shown in Figures 6 and 7 reveal well-crystallized AZO films with a rougher, more textured surface than those in Figure 3. The corresponding average rms roughness in a $3 \times 3\ \mu m^2$ area steadily increases from 15.1 to 40.2 nm with an increase of sputtering power from 80 to 140 W, as listed in Table 2. The morphology and roughness of such a textured surface of the AZO films are comparable to those made from acid-etched sputtering (11) or LPCVD methods (8).

During the two-step sputtering process, the growth of the overlayer and the surface texture is greatly influenced by the sputtering power, as is evident from the XRD patterns of the as-prepared one- and two-step AZO films in Figure 8. Under the same deposition conditions of 100 W and 0.2 Pa, the two-step sputtering achieved much better-crystallized and rougher surface-textured films, as is illustrated in Tables 1 and 2. The crystallinity of the as-deposited films can be indexed by the peak intensity and full width at half-maximum (fwhm) of the (002) diffraction peak. The well-crystallized polycrystalline film with large grains usually has strong diffraction peaks and a narrow fwhm. As shown in Figure 8, with increasing sputtering power, the (002) peak intensity dramatically increases and the fwhm decreases, which indicates the better-crystallized film obtained at a higher sputtering power. Because all of the SEM images (Figure 6) show a pyramidal microstructure on the surface, it is clear that crystal growth of the overlayer proceeded by advancing faceted fronts around the [001] axis, which is also supported by the previous XRD and SAED patterns in Figure 5.

A microstructure comparison of the films obtained by two- and one-step sputtering is seen in Figure 9, showing cross-sectional SEM images of two films. There is obvious columnar growth in the overlayer (Figure 9b) in two-step sputtering, but even in one-step sputtering, the growth eventually becomes columnar (Figure 9a), as is schematically illustrated on the right-hand side of Figure 9 (19, 20). However, as the power is increased in the second step, the diameter of the column increases (see Figure 6), reaching 500 nm in Figure 9b for 120 W. This compares with the seed crystal diameter of 50−100 nm (Figure 5b). Such columnar growth with increasing diameters occurs because the faster growing grains tend to crowd out the slower growing grains when they all compete in the same growth direction. Because a higher power promotes faster growth in general, it also favors the selection of the fastest growing grains. Therefore, the advantage of two-step sputtering lies in (i) nucleation of a coat of smaller seed crystals that provide a more complete coverage of the substrate and more crystals to select for later fast growth and (ii) faster growth conditions that favor fewer columns that grow to larger diameters while maintaining conformal coverage. As a result, a more coherent yet rougher surface-textured film results.

The electrical properties, including the resistivity, carrier concentration, and Hall mobility, were measured at room temperature and are listed in Table 2, and five excellent TCO films reported in the literature are also included in the table (8, 11, 17, 20). As the sputtering power is increased, the electrical resistivity and square resistance decreases from 5.16 Ω and $4.86 \times 10^{-4}\ \Omega \cdot cm$ to 0.66 Ω and $1.32 \times 10^{-4}\ \Omega \cdot cm$, respectively, which may be attributed to the increasing grain size and better crystallization achieved at higher power. The correlation between the mobility and sputtering power, however, is less clear. The mobility initially increases

Table 2. Physical Properties of the Two-Step Sputtered AZO Films and Five Excellent TCO Films Reported in the Literature

sample	thickness (μm)	rms roughness (nm)	haze at 360 nm (%)	growth temperature (K)	$R_{\square}$ (Ω/sq)	ρ ($\times 10^{-4}$ $\Omega \cdot$ cm)	μ (cm^2/V $\cdot$ s)	N ($\times 10^{21}$ cm^{-3})
1.2 Pa/60 W/10 min 0.2 Pa/80 W/40 min	1.16 ± 0.02	15.1 ± 0.3	31.1 ± 0.37	RT	5.16 ± 0.17	4.86 ± 0.12	6.68 ± 0.11	1.93 ± 0.14
1.2 Pa/60 W/10 min 0.2 Pa/100 W/30 min	1.48 ± 0.03	20.1 ± 0.36	49.8 ± 0.52	RT	1.45 ± 0.06	2.06 ± 0.15	15.2 ± 0.22	2.01 ± 0.2
1.2 Pa/60 W/10 min 0.2 Pa/120 W/25 min	1.56 ± 0.03	37.3 ± 0.41	53.7 ± 0.39	RT	0.9 ± 0.05	1.62 ± 0.06	35.4 ± 0.37	1.09 ± 0.04
1.2 Pa/60 W/10 min 0.2 Pa/140 W/20 min	1.63 ± 0.03	40.2 ± 0.28	60.7 ± 0.43	RT	0.66 ± 0.02	1.32 ± 0.09	26.3 ± 0.25	1.8 ± 0.15
ZnO:B LPCVD (8)	2.0−2.5		~60	453		110		
ZnO:Al sputtering + wet-etching (11)	1.20	2.8	70	573		3.8		
ZnO:Al RE-HSC (17)	1.03		~40	573	2.77	2.86	49.5	0.44
ZnO:Al PE-MOCVD (20)	0.94	41		473		3.0	~12.5	0.12
SnO_2:F CVD (17)	0.56		~35	~723	14.35	8.6	30.6	0.24

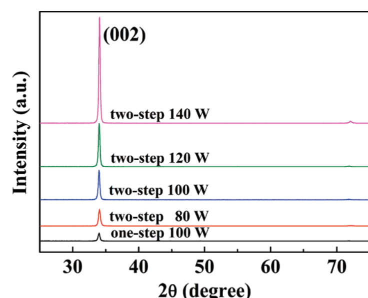

FIGURE 8. XRD patterns of AZO films deposited by one-step 100 W sputtering and two-step 80 W, 100 W, 120 W, and 140 W sputtering.

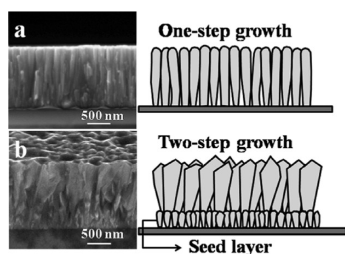

FIGURE 9. SEM images of the cross sections of (a) a one-step 100-W-deposited AZO film and (b) a two-step 120-W-deposited AZO film. Related schematic growth models of (a) one-step and (b) two-step AZO films are also shown.

with the power, peaking at 120 W with the highest mobility of 35.4 cm^2/V $\cdot$ s, and then decreases somewhat at 140 W. The carrier concentration is relatively insensitive to the power, but all are higher than 10^{21} cm^{-3}. These somewhat complicated correlations are not entirely surprising because the mobility and conductivity in thin films are sensitive to not only the crystal imperfection but also the surface roughness, which increases with the sputtering power. The lowest resistivity of 1.32×10^{-4} $\Omega \cdot$ cm achieved in the 140 W film is comparable to that of ITO films.

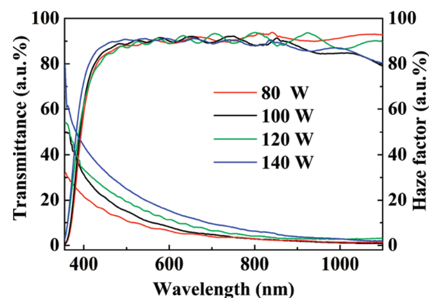

FIGURE 10. Transmittance and haze spectra of two-step sputtered AZO films deposited with the four different supplied powers.

The optical properties of the two-step sputtered AZO films are shown in Figure 10 and Table 2, which also includes other films in the literature for comparison. All of the as-deposited samples show a very similar transmittance in the entire spectral range in Figure 10. The average transmittance in 400−800 nm is between 85% and 90% and remains very high for the near-IR range. The 80 W film has a higher transmittance because of its thinner thickness. The higher transmittance of the 120 W film, especially in the near-IR region, is consistent with its lowest carrier concentration, which depresses the plasma frequency. Last, the haze factor increases with increasing power, as was expected from the rougher textured surface shown in Figure 6.

The main purpose of this study is to develop a simple magnetron sputtering method at room temperature to fabricate surface-textured AZO films to manage the incoming light. For the 140-W-deposited AZO films, a high-quality textured surface was obtained with a maximum haze factor of 60.7% at 360 nm and an average haze factor of 14.8% in the range of 360−1100 nm. In contrast to our results, the typical Asahi-U with textured FTO films has an average haze factor of about 15%, a sheet resistance of 6 Ω/sq, and a resistivity of 8.59×10^{-4} $\Omega \cdot$ cm, respectively (21). The BZO

ARTICLE

films with thicknesses of several micrometers have an electrical resistivity of $\sim 10^{-3}\ \Omega \cdot cm$, a haze factor of about 60%, and a transmittance of about 80% (8). In summary, the low conductivity, high transmittance, and high haze factor of our films compare favorably with the best TCO films in the literature, as is evident from Table 2.

4. CONCLUSIONS

A simple magnetron sputtering method at room temperature has been developed for producing transparent (transmittance above 85%) conducting (resistivity of $1.32 \times 10^{-4}\ \Omega \cdot cm$, square resistance of <0.66 Ω/sq) Al-doped ZnO films with a high haze factor (60%) that are advantageous for solar cell applications. A two-step mechanism of film growth to deposit surface-textured TCO films has been proposed. The two-step method provides a seed layer with 50−100 nm (002)-textured grains from which large (500 nm) columnar, front-faceted grains can grow selectively in the second step, providing coherent films with faceted rough surfaces (with a maximum rms roughness of 40.2 nm). The use of a zinc-rich sputtering target low-temperature-sintered from coprecipitated powders is advantageous; further studies are required to understand its role in AZO film deposition and film quality. The simplicity of the present method and the superior electrical and optical properties of the films may allow surface-textured AZO films to be produced at low cost on an industrial scale for commercial applications.

Acknowledgment. Financial support from the National 973 Program of China (Grants 2007CB936704 and 2009CB939903), National Science Foundation of China (Grants 50772123 and 10775171), and Science and Technology Commission of Shanghai (Grants 10520706700 and 0952nm06500) is acknowledged.

REFERENCES AND NOTES

(1) Woodcock, J. M.; Schade, H.; Maurus, H.; Dimmler, B.; Springer, J.; Ricaud, A. In *Proceedings of the 14th European Photovoltaic Solar Energy Conference*, Barcelona, Spain, 1997; Ossenbrink, H. A., Helm, P., Ehmann, H., Eds.; Stephans: Bedford, U.K., 1997; pp 857−860.

(2) Mutitu, J. G.; Shi, S. Y.; Chen, C. H.; Creazzo, T.; Barnett, A.; Honsberg, C.; Prather, D. W. *Opt. Express* **2008**, *16*, 15238–15248.

(3) Granqvist, C. G. *Thin Solid Films* **1990**, *193−194*, 730–741.

(4) Ginley, D. S.; Bright, C. *MRS Bull.* **2000**, *25*, 15–18.

(5) Kim, H.; Horwitz, J. S.; Kushto, G. P.; Kafafi, Z. H.; Chrisey, D. B. *Appl. Phys. Lett.* **2001**, *79*, 284–286.

(6) Faÿ, S.; Dubail, S.; Kroll, U.; Meier, J.; Ziegler, Y.; Shah, A. In *Proceedings of the 16th European Photovoltaic Solar Energy Conference*, Glasgow, U.K., 2000;Scheer, H., McNelis, B., Palz, W., Ossenbrink, H. A., Helm, P., Eds.; 2000; pp 361−364.

(7) Van den Berg, R.; Calwer, H.; Marklstorfer, P.; Meckes, R.; Schulze, F. W.; Ufert, K. D.; Vogt, H. *Sol. Energy Mater. Sol. Cells* **1993**, *31*, 253–261.

(8) Faÿ, S.; Kroll, U.; Bucher, C.; Vallat-Sauvain, E.; Shah, A. *Sol. Energy Mater. Sol. Cells* **2005**, *86*, 385–397.

(9) Selvan, J. A. A. Ph.D. Thesis, Universite de Neuchatel, Neuchatel, Switzerland, 1998; ISBN 3-930803-60-7.

(10) Kluth, O.; Loffl, A.; Wieder, S.; Beneking, C.; Appenzeller, W.; Houben, L.; Rech, B.; Wagner, H.; Hoffmann, S.; Waser, R.; Selvan, J. A. A.; Keppner, H. *Proceedings of the 26th IEEE Photovoltaic Specialists Conference*, Anaheim, CA, 1997; IEEE: New York, 1997; pp 715−718.

(11) Yoo, J.; Lee, J.; Kim, S.; Yoon, K.; Park, I. J.; Dhungel, S. K.; Karunagaran, B.; Mangalaraj, D.; Yi, J. *Thin Solid Films* **2005**, *480−481*, 213–217.

(12) Tohsophon, T.; Hüpkes, J.; Siekmann, H.; Rech, B.; Schultheis, M.; Sirikulrat, N. *Thin Solid Films* **2008**, *516*, 4628–4632.

(13) Ip, K.; Baik, K. H.; Overberg, M. E.; Lambers, E. S.; Heo, Y. W.; Norton, D. P.; Pearton, S. J.; Ren, F.; Zavada, J. M. *Appl. Phys. Lett.* **2002**, *81*, 3546–3548.

(14) Bae, J. W.; Jeong, C. H.; Kim, H. K.; Kim, K. K.; Cho, N. G.; Seong, T. Y.; Park, S. J.; Adesida, I.; Yeom, G. Y. *Jpn. J. Appl. Phys.* **2003**, *42*, L535–L537.

(15) Lim, W. T.; Baek, I. K.; Lee, J. W.; Lee, E. S.; Jeon, M. H.; Cho, G. S.; Heo, Y. W.; Norton, D. P.; Pearton, S. J. *Appl. Phys. Lett.* **2003**, *83*, 3105–3107.

(16) Agashe, C.; Kluth, O.; Hupkes, J.; Zastrow, U.; Rech, B. *J. Appl. Phys.* **2004**, *95*, 1911–1917.

(17) Guo, S.; Patel, A.; Cambridge, J.; Stavrides, A.; Le, L. T.; Efstathiadis, H.; Haldar, P.; Delahoy, A. E. *23rd European Photovoltaic Solar Energy Conference and Exhibition*; Valencia, Spain, 2008; pp 2482−2485.

(18) Duenow, J. N.; Gessert, T. A.; Wood, D. W.; Young, D. L. *J. Non-Cryst. Solids* **2008**, *354*, 2787–2790.

(19) Xiao, R. F.; Alexander, J. I. D.; Rosenberger, F. *Phys. Rev. A* **1991**, *43*, 2977–2992.

(20) Volintiru, I.; Creatore, M.; Kniknie, B. J.; Spee, C. I. M. A.; van de Sanden, M. C. M. *J. Appl. Phys.* **2007**, *102*, 043709-1–043709-9.

(21) Sato, K.; Gotoh, Y.; Wakayama, Y.; Hayashi, Y.; Adachi, K.; Nishimura, H. *Asahi Garasu Kenkyu Hokoku* **1992**, *42*, 129–137.

AM100416E